Skin-Integrated Electromechanical Systems for Characterization of Deep Tissue Biomechanics

Enming Song,[1,2,16] Zhaoqian Xie,[3,16] Wubin Bai,[1,4,16] Haiwen Luan,[1,16] Bowen Ji,[5] Xin Ning,[6] Yu Xia,[7] Janice Mihyun Baek,[7] Yujin Lee,[7] Raudel Avila,[8] Huang-Yu Chen,[1] Jae Hwan Kim,[7] Surabhi Madhvapathi,[1] Kuanming Yao,[2] Sang Min Won,[9] Xinyuan Zhang,[10] Daniel J. Myers,[1,11] Yongfeng Mei,[10] Xu Guo,[3] Shuai Xu,[1,11] Xinge Yu,[2*] Yonggang Huang, [8,12,13*] and John A. Rogers[1,8,13,14,15*]

[1] Querrey Simpson Institute for Bioelectronics, Northwestern University, Evanston, IL 60208, USA;

[2] Department of Biomedical Engineering, City University of Hong Kong, Hong Kong 999077, China;

[3] State Key Laboratory of Structural Analysis for Industrial Equipment, Department of Engineering Mechanics, Dalian University of Technology, Dalian 116024, China;

[4] Department of Applied Physical Sciences, University of North Carolina at Chapel Hill, Chapel Hill, NC 27599, USA;

[5] Unmanned System Research Institute, Northwestern Polytechnical University, Xi'an 710072, China

[6] Department of Aerospace Engineering, The Pennsylvania State University, University Park, PA 16802, USA;

[7] Frederick Seitz Materials Research Laboratory, University of Illinois at Urbana-Champaign, Urbana, IL 61801, USA;

[8] Department of Mechanical Engineering, Northwestern University, Evanston, IL 60208, USA;

[9] Department of Electrical and Computer Engineering, Sungkyunkwan University, Suwon 16419, Republic of Korea;

[10] Department of Materials Science, State Key Laboratory of ASIC and Systems, Fudan University, Shanghai 200433, China;

[11] Department of Dermatology, Feinberg School of Medicine, Northwestern University, Chicago, IL 60611, United States;

[12] Department of Civil and Environmental Engineering, Northwestern University, Evanston, IL 60208, USA;

[13] Department of Materials Science and Engineering, Northwestern University, Evanston, IL 60208, USA;

[14] Department of Biomedical Engineering, Northwestern University, Evanston, IL 60208, USA;

[15] Department of Neurological Surgery, Northwestern University, Evanston, IL 60208, USA;

[16] These authors contributed equally to this work.

[*] To whom correspondence should be addressed. Email: xingeyu@cityu.edu.hk; y-huang@northwestern.edu; jrogers@northwestern.edu.

Keywords: skin-integrated electronics, biomechanics, biosensing, dermatology

Supplementary Information

Supplementary Note 1

Supplementary Legends of Figures, Table and Movie

Supplementary Figure S1-S23

Supplementary Table S1

Supplementary Movie S1

Supplementary Note 1:

Finite Element Analysis (FEA). The commercial software ABAQUS was used to study the mechanical interaction among the actuator, Au sensor and tissues to be measured. The PDMS, phantom tissues and magnet were modeled by hexahedron elements (C3D8R) while the thin Au and Polyimide film were modeled by composite shell elements (S4R). The minimal element size was 1/5 of the width of the narrowest interconnects (50 μm). The mesh convergence of the simulation was ensured for all cases. The elastic modulus (E), Poisson's ratio (v) and density (ρ) are E_{PDMS}=1MPa, v_{PDMS} =0.5, ρ_{PDMS}= 0.96×10^3 kg/m^3, E_{Au}=79 GPa, v_{Au} =0.4, ρ_{Au}=19.32×10^3 kg/m^3, E_{magnet}=113 GPa, v_{magnet}=0.34, and ρ_{magnet}=8.08×10^3 kg/m^3, E_{PI}=2.5 GPa, v_{PI}=0.34, ρ_{PI}=0.91×10^3 kg/m^3, E_{Cu}=119 GPa, v_{Cu}=0.32, and ρ_{Cu}=8.96×10^3 kg/m^3.

References

1. Yu, X. et al. Skin-integrated wireless haptic interfaces for virtual and augmented reality. *Nature* **575**, 473-479 (2019).

Supplementary Figure Legends

Figure S1. Steps for fabricating and assembling EMM sensors. 1. Formation of electrical interconnects and strain gauges on glass wafers; 2. Transfer-printing procedure with a water soluble tape; 3. Printing onto a flexible layer of PDMS; 4. Assembly of the sensor with mechanical actuators, connected via wires and a PCB.

Figure S2. The strain sensor consisting of two-terminal Au wire connection embedded in polyimide layer, with (**a**) circuit diagram and (**b**, **c**) optical images of different locations.

Figure S3. Measurement setup for mechanical sensing that includes a current source, a lock-in amplifier and EMM sensor with external connection and biological measurement targets.

Figure S4. Robust mechanical properties of (**a**), (**b**) the flexible sheets of strain gauges and (**c**) the systems assembled with actuators, indicating that the sensors can be bent (**a**) and twisted (**b**) and the entire system can laminate onto a curved surface (**c**).

Figure S5. (**a**) Sensor resistance as a function of cycles of bending. Inset is an optical image of the sensor on a surface with a radius of curvature of 1.5 cm. (**b**) Bending tests and accelerated soak tests of the strain sensor. Inset shows an image of a sensor immersed in artificial sweat at 50 ^{o}C.

Figure S6. Systematic studies of the bending effects of EMM sensor measurements. (**a**) EMM sensors coupled on cylindrical substrates of PDMS with radius of curvature of 4 cm, 8 cm, 10 cm and ∞ cm, respectively. (**b**) Sensing voltages of EMM sensors with different bending radius.

Figure S7. Statistics on the resistance (strain sensor), yield, and the *SNR* (during measurements on cheek) of 100 fabricated devices. The yield corresponds to the percentage of functional devices.

Figure S8. Applications of EMM sensors on human subjects. The system can be placed in contact with various locations of human body such as the (**a**) forearm and (**b**) shoulder. An adhesive film (3M Tegaderm Film) laminated on top of the entire structure prevents motion during measurements.

Figure S9. Normalized amplitude-frequency response of the vibratory actuator in contact with an artificial skin sample with an modulus of 200 kPa.

Figure S10. (**a**) Schematic diagram of an EMM sensor coupled onto artificial skin samples (PDMS layers) on glass substrates, as an approximate mimic of the structure of device/skin/bones. (**b**) A collection of measurements of elastic modulus on different PDMS layers, as function of weight ratios of crosslinker, all tested by the commercial bio-indenter.

Figure S11. Recording of sensing voltages of V_S as function of actuation frequencies on artificial skin samples with elastic moduli of 200 kPa, without the magnets.

Figure S12. Simulated (line) and measured (symbols) V_S as a function of elastic modulus of the PDMS sample at 50 Hz, with constant thickness of 8 mm.

Figure S13. Results of experimental (E), FEA results and the fitting lines (Equation 1) of V_S as a function of sample thicknesses with various sample moduli.

Figure S14. Comparison of measurement results with EMM sensors on the same location of a human thigh with (**a**) hair bearing and (**b**) hairless regions. (**c**) The output sensing voltages show stable performance on both regions.

Figure S15. Schematic illustration of a simulated patient test. EMM sensors are coupled onto a silicone substrate (1 cm thick), with modulus of 500 kPa for the central part (1 cm diameter) and of 100 kPa for the surrounding part of the substrate that mimics the structure of a skin tumor, in an exploded (**a**) and cross-sectional (**b**) view.

Figure S16. Measurement results of the simulated patient test in *SI Appendix*, Figure S15. Left: Photograph of the simulated patient test. Right: EMM sensor measurements of modulus values at the central and surrounding regions of the silicone substrate.

Figure S17. EMM measurements on (**a**) arm (**b**) hand and (**c**) lower back, with sensors on psoriasis lesion (right) and on nearby skin under normal conditions (left). Black frames correspond to the lesion regions of psoriasis.

Figure S18. Experimental results for sensing voltages from EMM sensors with (**a**) 3 mm diameter and (**b**) 1.5 mm diameter magnets as function of the thickness of artificial skin samples.

Figure S19. Simple estimation of tissue thickness in fingertip dorsum, with length measurements (**a**) from bottom of fingertip to nail plate; and (**b**) from bottom of fingertip to fingertip dorsum near the nail plate. The combined thickness for skin/tissues of fingertip dorsum near the nail root is ~3 mm.

Figure S20. FEA modeling to determine the modulus of skin and inner tissues for (**a**) cheek region and (**b**) fingertip dorsum from measurements using EMM sensors with different D. Here, E_A and E_B correspond to elastic modulus for skin and inner tissues. Insets show the photographs of the measurements.

Figure S21. Photograph of the strain sensor array on a polymer substrate during bent status.

Figure S22. (**a**) Photograph of the final, complete EMM mapping array laminated on an artificial skin (PDMS, 2 cm thick). Interconnections use flexible cable of heat seal connectors (HSCs). (**b**) The connection of the EMM array system to an external multiplexing board.

Figure S23. Schematic illustration of the DAQ system.

Table S1. The relationship between the elastic modulus E of tissues and $C(E)$ in Equation 1.

Movie S1. The video captured using a high-speed camera for vibration of magnet in slow motion at 50 Hz and V_A of 5 V.

Figure S1

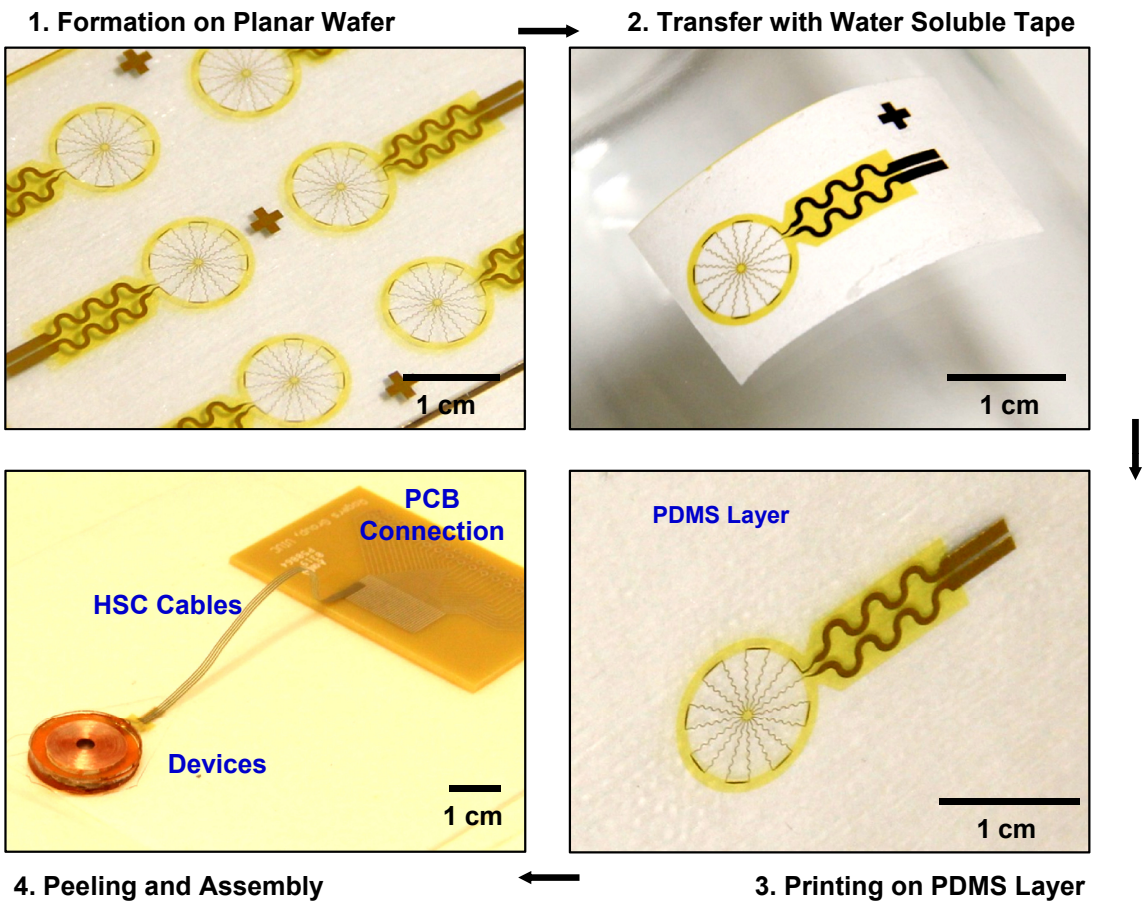
1. Formation on Planar Wafer
2. Transfer with Water Soluble Tape
1 cm
1 cm
PCB
Connection
HSC Cables
Devices
1 cm
PDMS Layer
1 cm
4. Peeling and Assembly
3. Printing on PDMS Layer

Figure S2

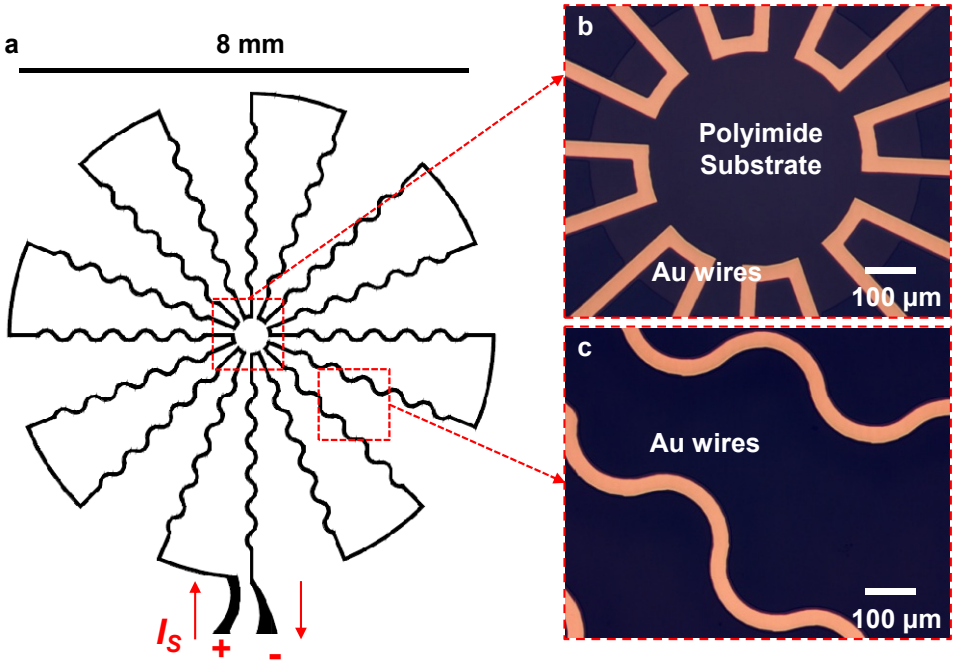
a
8 mm
I_S
+
-
b
Polyimide
Substrate
Au wires
100 μm
c
Au wires
100 μm

Figure S3

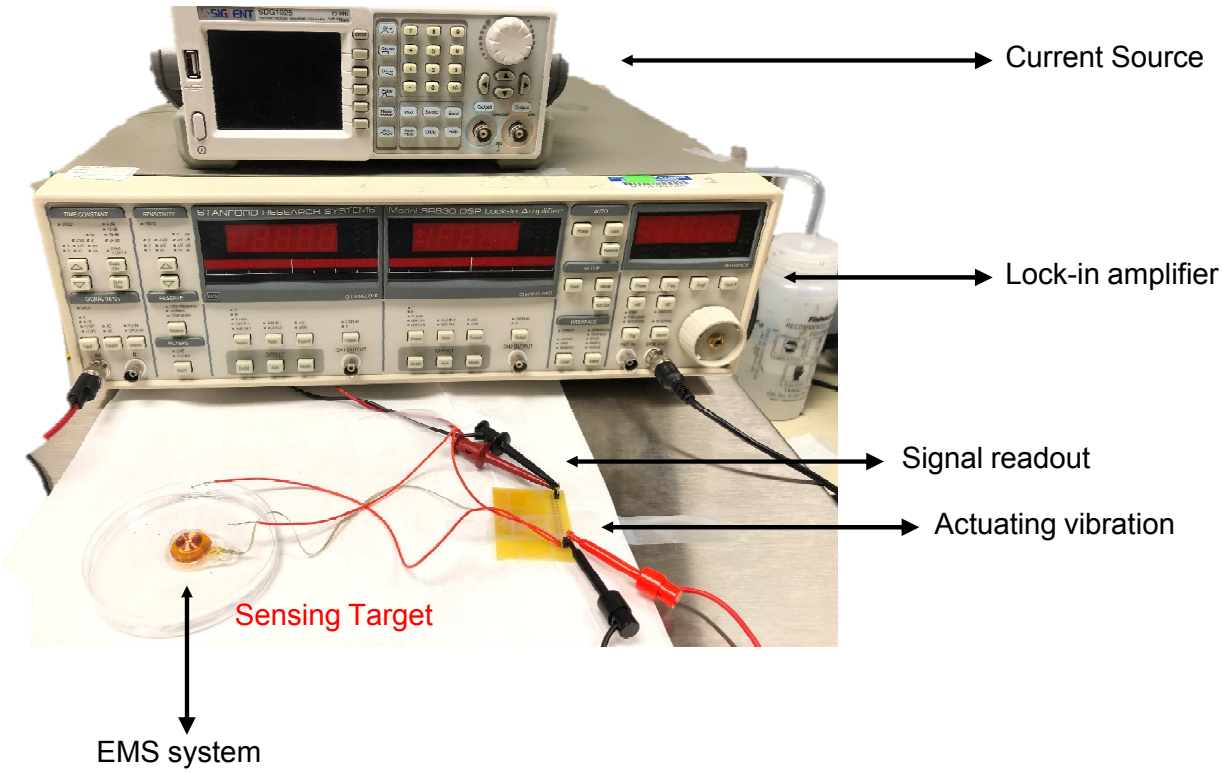
Current Source
Lock-in amplifier
Signal readout
Actuating vibration
Sensing Target
EMS system

Figure S4

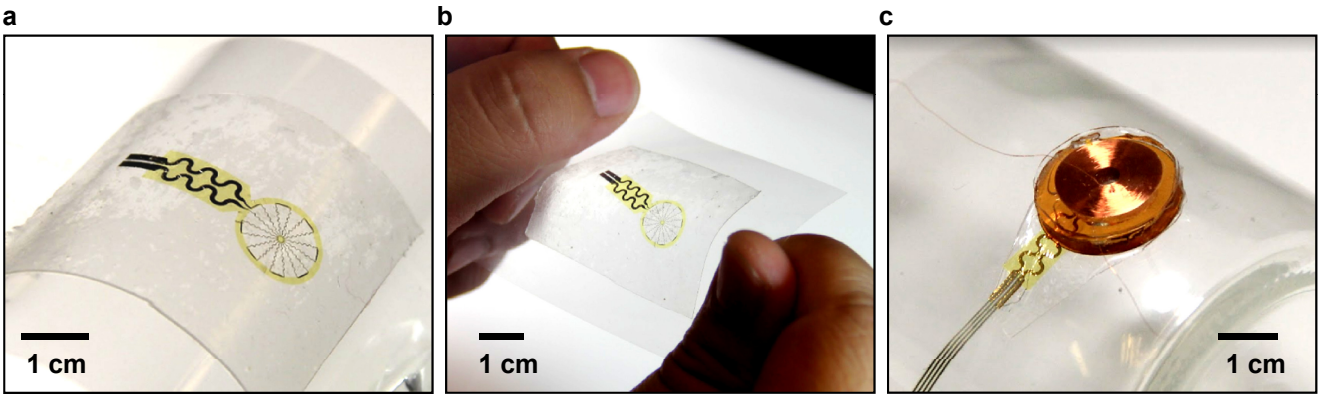

Figure S5

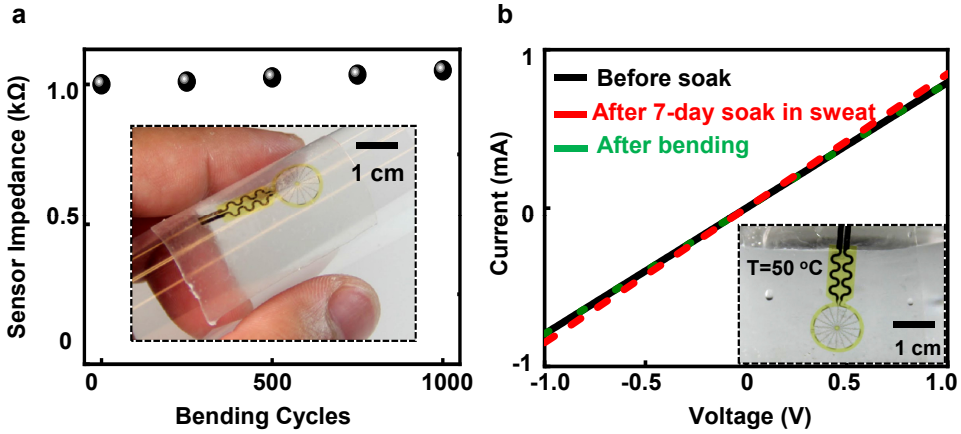
a
Sensor Impedance (kΩ)
1.0
0.5
0
0
500
1000
Bending Cycles
1 cm
b
Current (mA)
1
0
-1
-1.0
-0.5
0
0.5
1.0
Voltage (V)
Before soak
After 7-day soak in sweat
After bending
T=50 °C
1 cm

Figure S6

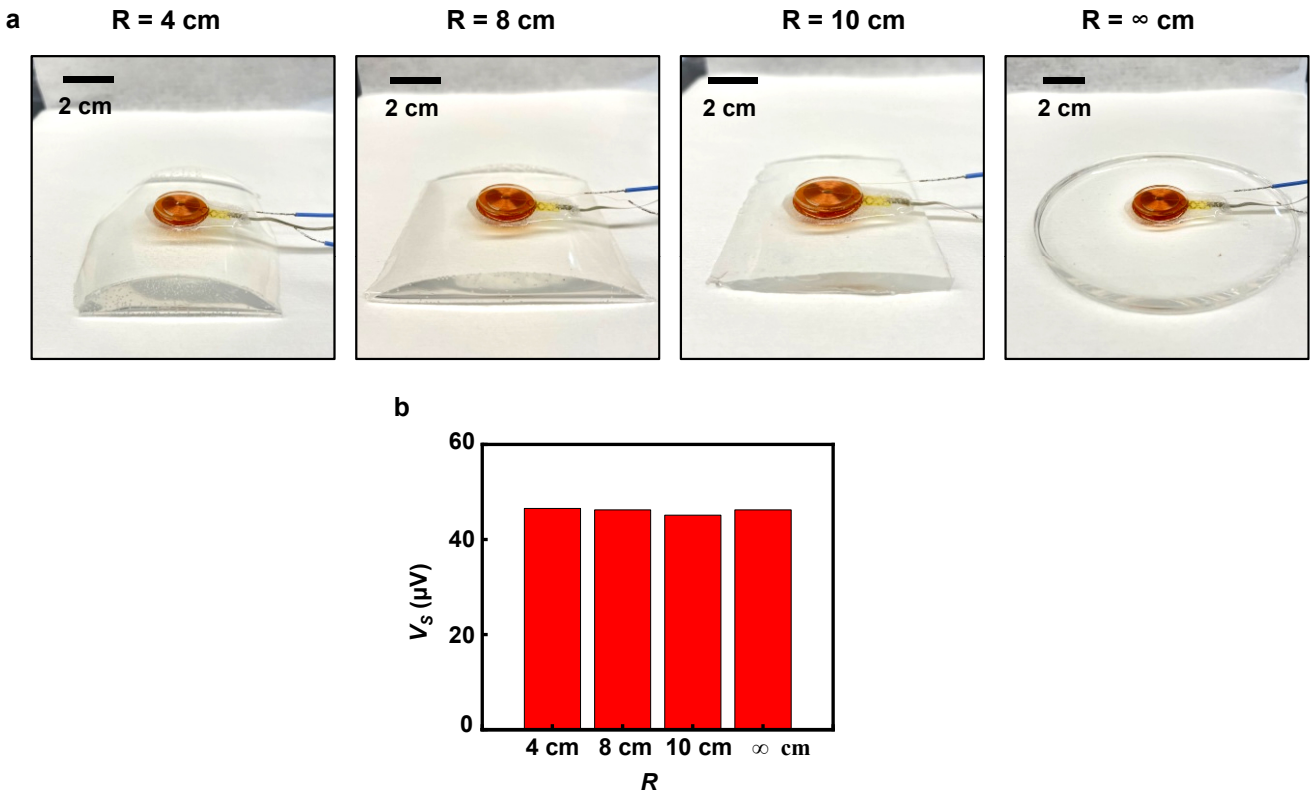
a
R = 4 cm
R = 8 cm
R = 10 cm
R = ∞ cm
2 cm
2 cm
2 cm
2 cm
b
60
40
20
0
V_S (μV)
4 cm
8 cm
10 cm
∞ cm
R

Figure S7

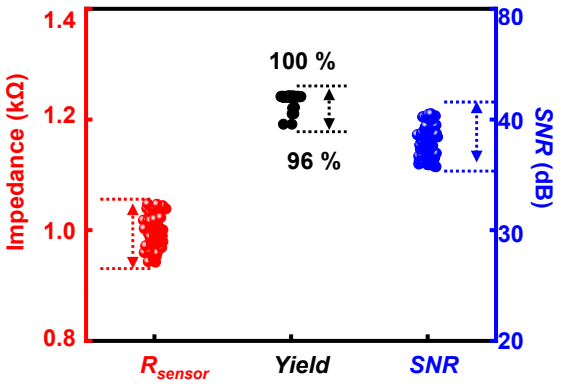
1.4
1.2
1.0
0.8
Impedance (kΩ)
80
40
30
20
SNR (dB)
100 %
96 %
R_sensor
Yield
SNR

Figure S8

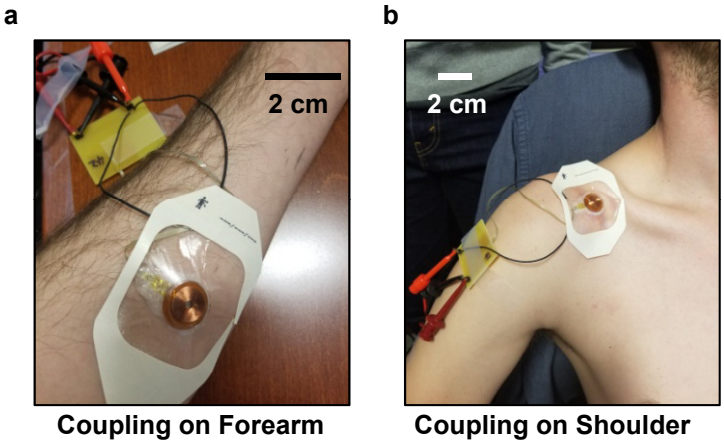

Figure S9

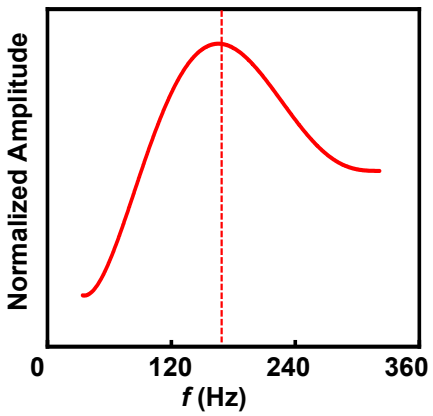

Figure S10

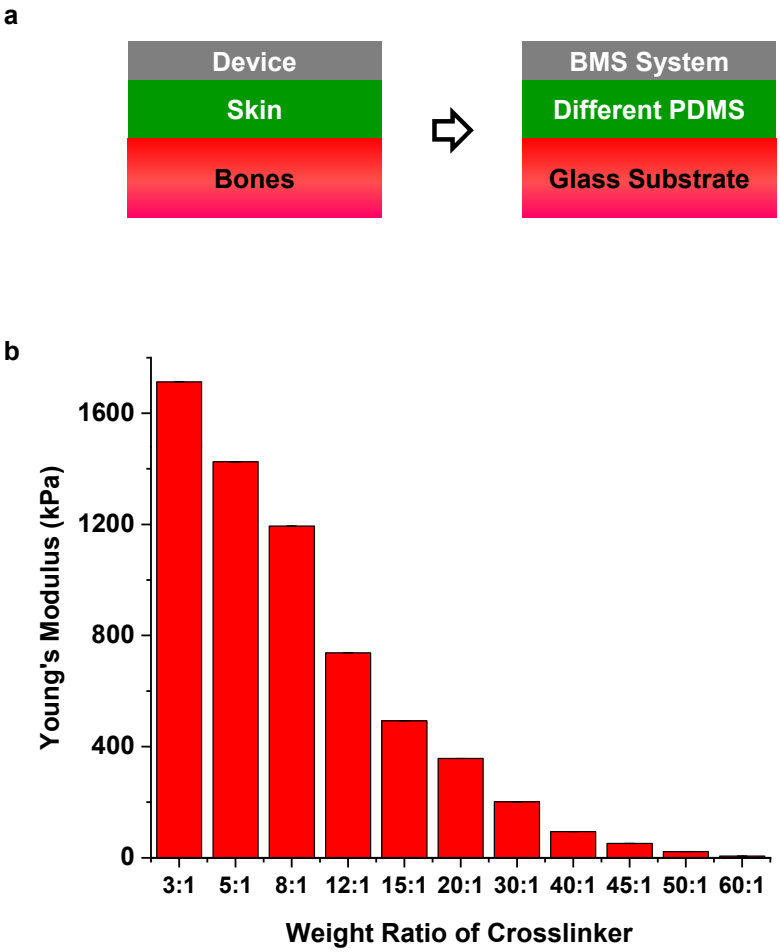
a
Device
Skin
Bones
BMS System
Different PDMS
Glass Substrate
b
Young's Modulus (kPa)
1600
1200
800
400
0
3:1
5:1
8:1
12:1
15:1
20:1
30:1
40:1
45:1
50:1
60:1
Weight Ratio of Crosslinker

Figure S11

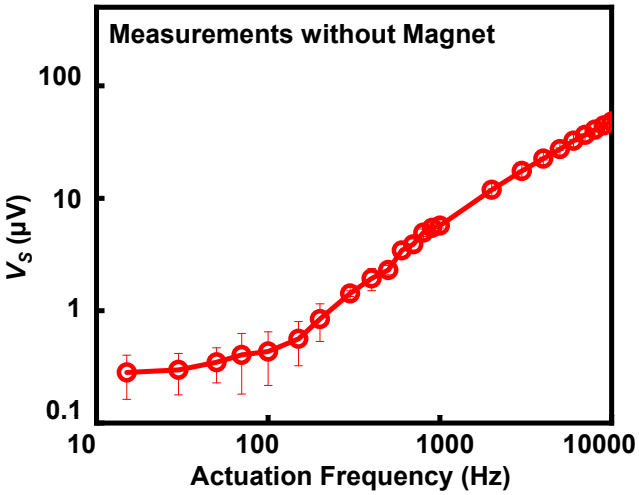
Measurements without Magnet
100
10
1
0.1
V_S (μV)
10
100
1000
10000
Actuation Frequency (Hz)

Figure S12

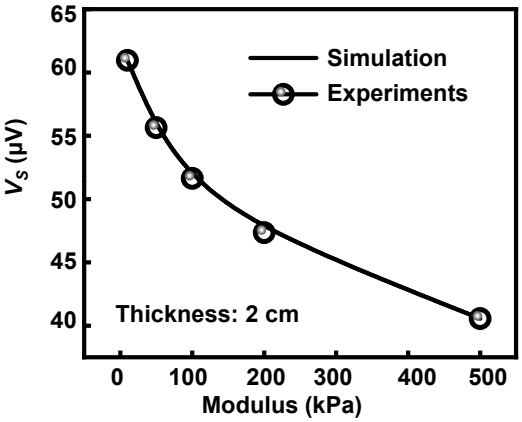
65
60
55
50
45
40
V_S (μV)
Simulation
Experiments
Thickness: 2 cm
0
100
200
300
400
500
Modulus (kPa)

Figure S13

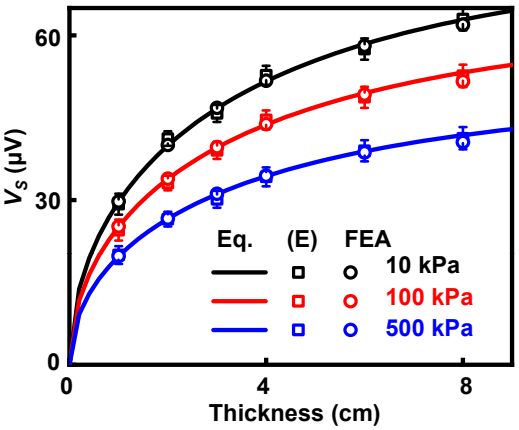

Figure S14

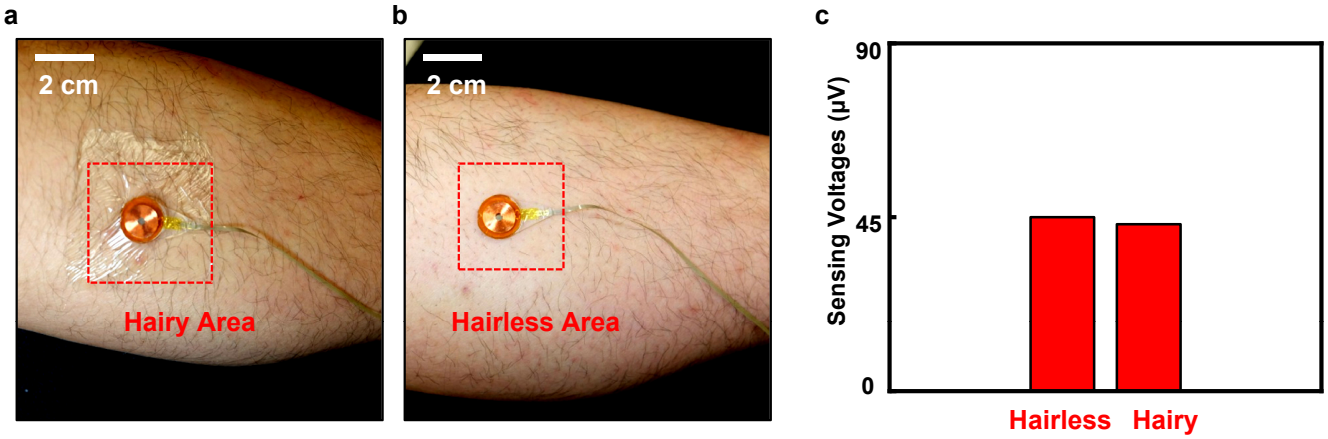
a
2 cm
Hairy Area
b
2 cm
Hairless Area
c
Sensing Voltages (μV)
90
45
0
Hairless
Hairy

Figure S15

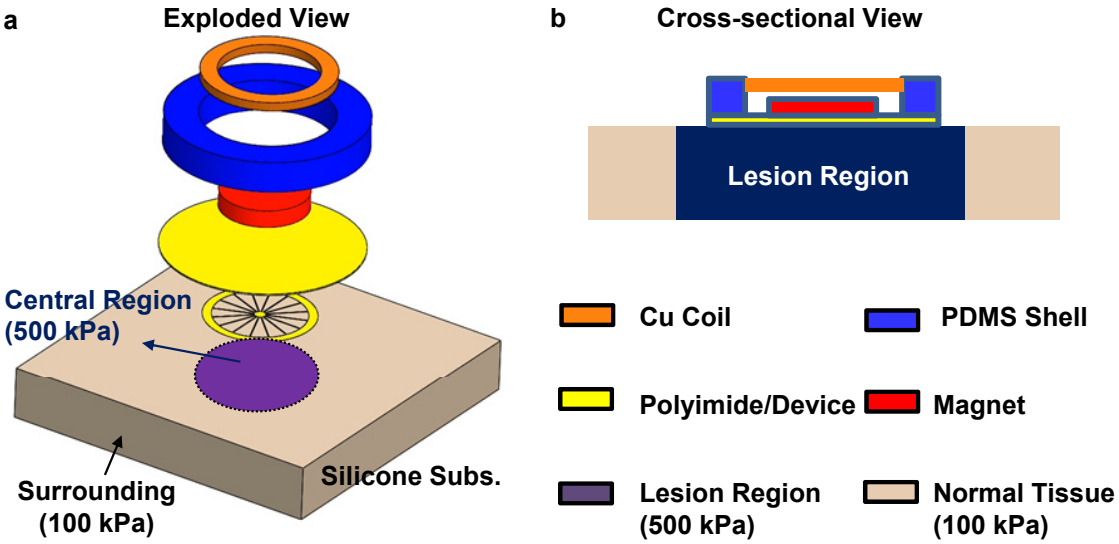
a
Exploded View
Central Region
(500 kPa)
Surrounding
(100 kPa)
Silicone Subs.
b
Cross-sectional View
Lesion Region
Cu Coil
PDMS Shell
Polyimide/Device
Magnet
Lesion Region
(500 kPa)
Normal Tissue
(100 kPa)

Figure S16

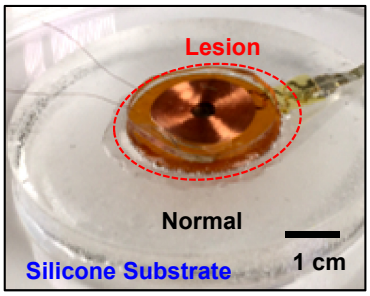
Lesion
Normal
Silicone Substrate
1 cm

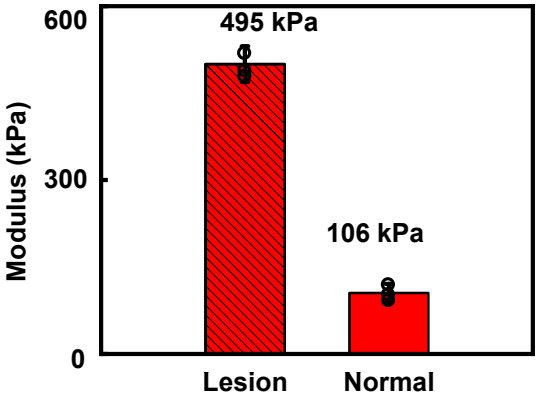
600
300
0
Modulus (kPa)
495 kPa
106 kPa
Lesion
Normal

Figure S17

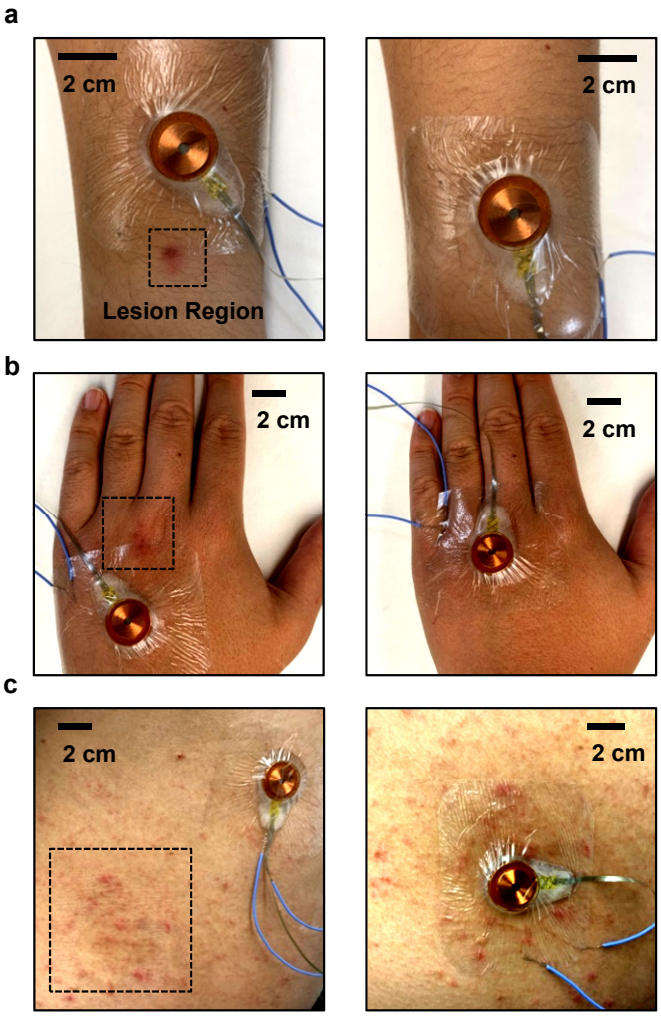

Figure S18

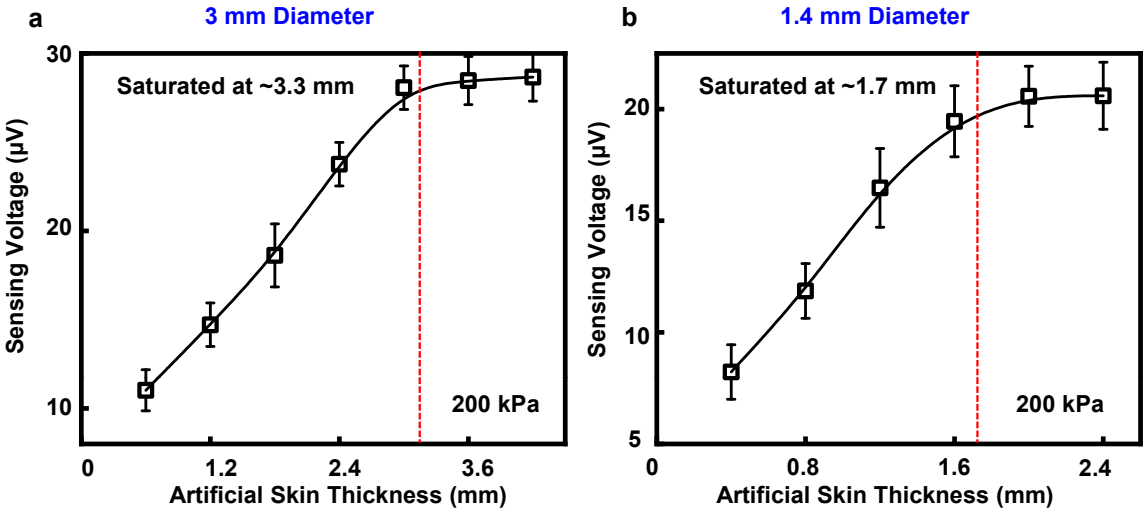
a
3 mm Diameter
Saturated at ~3.3 mm
200 kPa
Sensing Voltage (μV)
Artificial Skin Thickness (mm)
30
20
10
0
1.2
2.4
3.6
b
1.4 mm Diameter
Saturated at ~1.7 mm
200 kPa
Sensing Voltage (μV)
Artificial Skin Thickness (mm)
20
15
10
5
0
0.8
1.6
2.4

Figure S19

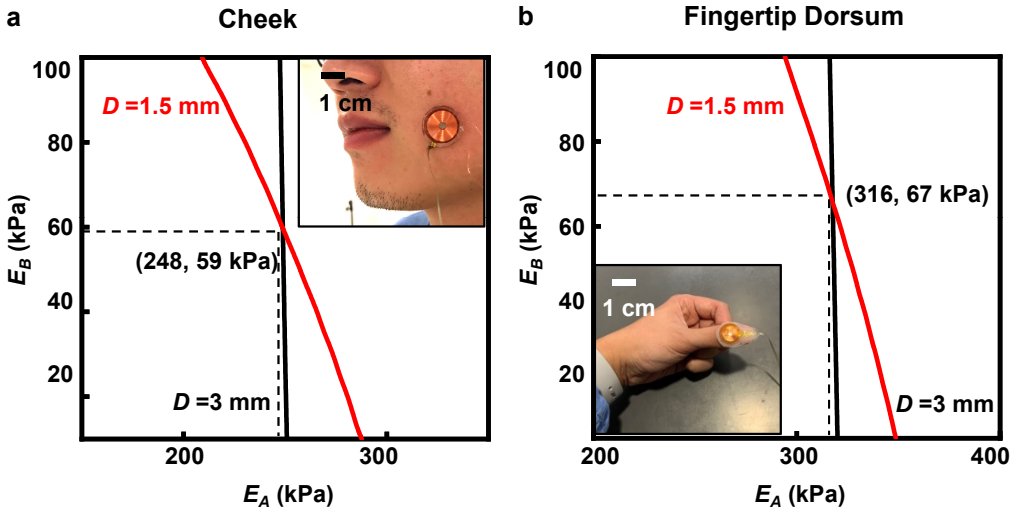
a
Cheek
100
80
60
40
20
E_B (kPa)
D =1.5 mm
1 cm
(248, 59 kPa)
D =3 mm
200
300
E_A (kPa)
b
Fingertip Dorsum
100
80
60
40
20
E_B (kPa)
D =1.5 mm
(316, 67 kPa)
1 cm
D =3 mm
200
300
400
E_A (kPa)

Figure S20

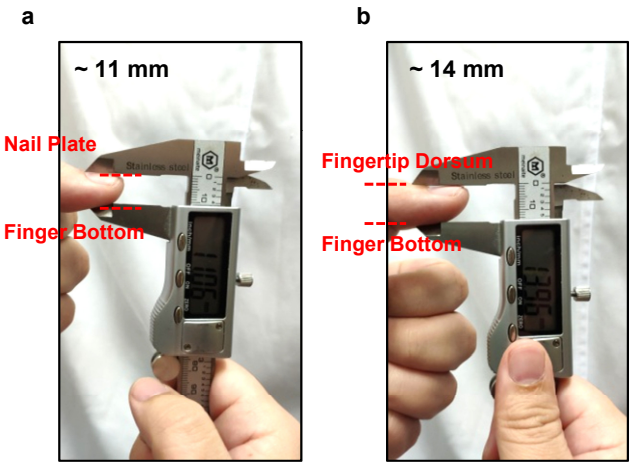
a
~ 11 mm
Nail Plate
Finger Bottom
b
~ 14 mm
Fingertip Dorsum
Finger Bottom

Figure S21

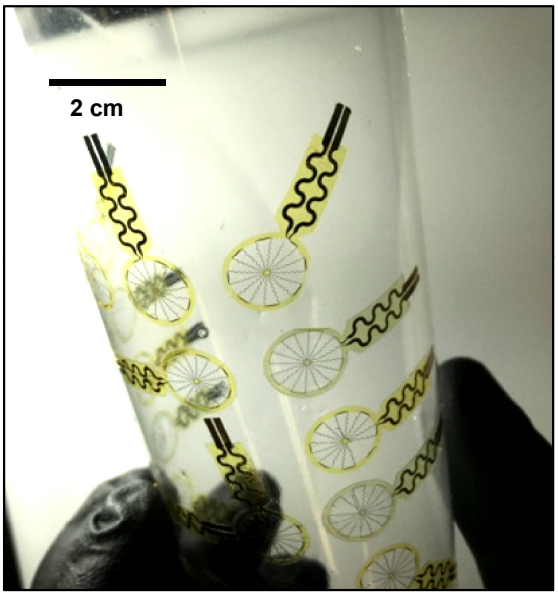

Figure S22

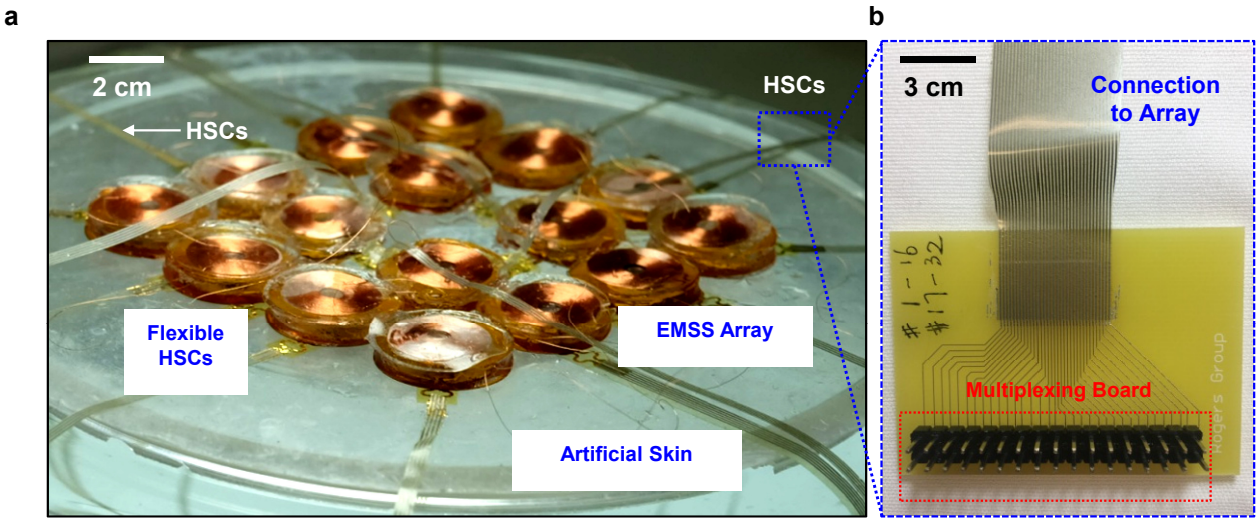
a
b
2 cm
HSCs
HSCs
Flexible HSCs
EMSS Array
Artificial Skin
3 cm
Connection to Array
Multiplexing Board

Figure S23

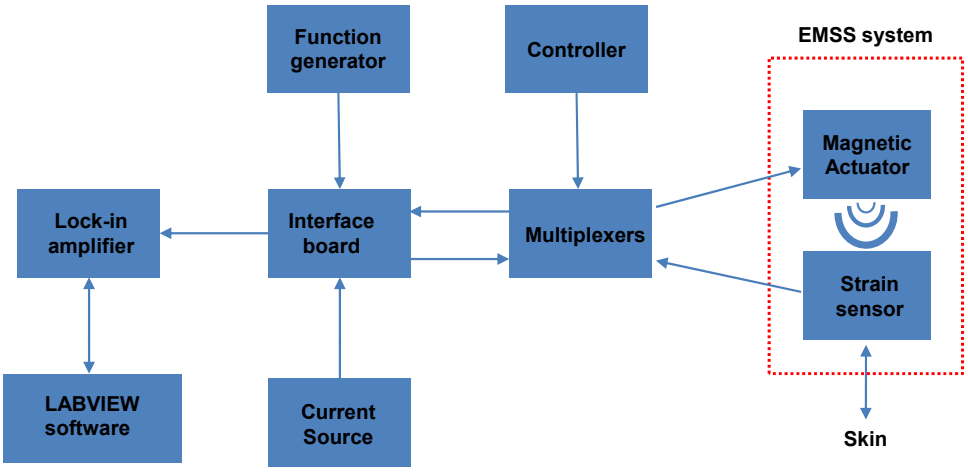
Function generator
Controller
EMSS system
Magnetic Actuator
Lock-in amplifier
Interface board
Multiplexers
Strain sensor
LABVIEW software
Current Source
Skin

Table S1

E (kPa)	C(E)
10	1.53E-05
100	1.30E-05
500	1.02E-05

Table S1. The relationship between the elastic modulus E and C(E) in Equation 1.